



# Formation, characterization and electrochemical properties of novel tetrasubstituted cobalt phthalocyanines bearing tetrahydropyran, furan and coumarin moieties



Sumayya Chohan, Irvin Noel Booyesen\*, Allen Mambanda, Matthew Piers Akerman

University of KwaZulu-Natal, School of Chemistry and Physics, Private Bag X01, Scottsville 3209, Pietermaritzburg, South Africa

## ARTICLE INFO

### Article history:

Received 18 February 2016  
Received in revised form 10 April 2016  
Accepted 11 April 2016  
Available online 20 April 2016

### Keywords:

Metallophthalocyanine  
Tetrahydropyran  
Furan  
Spectroelectrochemistry  
Electrocatalysis  
L-Cysteine

## ABSTRACT

Cobalt phthalocyanines (CoPcs) bearing peripherally tetrasubstituted tetrahydropyran (thp) or furan (fur) moieties were formed and spectroscopically characterized. Structural elucidations of 4-(tetrahydropyran-2-methoxy)phthalonitrile (**1**) and 4-(furan-2-methylthio)phthalonitrile (**2**) were confirmed *via* single crystal X-ray analysis. The redox properties of CoPc-thp (**3**) and CoPc-fur (**4**) were investigated *via* cyclic and squarewave voltammetry as well as UV–Vis spectroelectrochemistry. Glassy carbon electrodes (GCEs) modified with **3**, **4** and a previously reported coumarin (cou) substituted CoPc (CoPc-cou, **5**), were tested for their electrocatalytic activities toward L-cysteine. While the bare GCE and **4**-GCE showed no peaks for L-cysteine oxidation in the 0.0–0.70 V potential window; **3**-GCE and **5**-GCE showed peaks at 0.42 V and 0.52 V, respectively. Kinetic parameters were determined by chronoamperometry studies. L-Cysteine oxidation using **3**-GCE was found to proceed at a faster rate than **5**-GCE.

© 2016 Elsevier B.V. All rights reserved.

## 1. Introduction

L-Cysteine is an amino acid that plays a crucial role in biological systems for the functioning of various proteins [1]. It has several applications in the pharmaceutical and food industries for the formulation of drugs and the production of antibiotics and antioxidants [2]. A deficiency in L-cysteine is associated with many health issues such as liver damage, skin lesions, hair depigmentation and muscle loss; hence, its detection is of great importance for physiological and clinical diagnosis [3,4]. Electrochemical methods have proved to be the preferred choice for this purpose above other techniques like chromatographic separation and spectrometric methods [5,6] due to their simplicity, enhanced selectivity and high sensitivity [7]. The detection of L-cysteine on bare electrodes requires high overpotentials which results in sluggish responses, surface fouling and interference from other analytes [3,7,8]. To overcome these shortcomings, researchers are focusing on the development of chemically modified electrodes (CMEs) to electrocatalytically enhance the detection of L-cysteine [9,10].

Metallophthalocyanines (MPcs) are versatile materials that are particularly useful in the preparation of biosensors [11–13]. The

high chemical, thermal and mechanical stability of these metal complexes makes them an attractive choice for such application [14,15]. In many instances, electrodes modified with MPcs have shown excellent electrocatalytic behavior towards various biologically important analytes [16,17]. MPc modified electrodes can be prepared in various ways such as the drop-dry method, formation of Langmuir–Blodgett films, self-assembled monolayers, electropolymerization and electrodeposition [18–21].

Optimization of the electrochemical properties of MPcs can be achieved by modification of the substituents and/or metal centres [22,23]. Redox active metal centres like Co, Fe and Mn promote electron mediation [24] while biosensors prepared with MPcs containing biologically active substituents have been reported to show improved selectivity and sensitivity towards biological analytes [25,26]. Furan derivatives are known to possess anti-bacterial, anti-tumor and analgesic properties [27,28] while pyrans have been discovered to have antimicrobial and antioxidant activities [29,30]. In this study, we report on the synthesis and characterization of CoPcs substituted with biologically relevant tetrahydropyran (thp) and furan (fur) moieties. In addition, we explore the comparative electrocatalytic capabilities of glassy carbon electrodes (GCEs) modified with MPcs containing thp and coumarin (cou) moieties, towards L-cysteine.

\* Corresponding author.

E-mail address: [Booyсени@ukzn.ac.za](mailto:Booyсени@ukzn.ac.za) (I.N. Booyesen).

## 2. Experimental

### 2.1. Materials

4-Nitrophthalonitrile, tetrahydropyran-2-methanol, 2-furan-methanethiol, potassium carbonate, cobalt(II) chloride, 1,8-diazabicyclo[5.4.0]undec-7-ene (DBU) and electrochemical analysis grade tetrabutylammoniumtetrafluoroborate (TBABF<sub>4</sub>) were purchased from Sigma–Aldrich and used without further purification. Organic solvents, phosphorus pentoxide (P<sub>2</sub>O<sub>5</sub>), molecular sieves (4 Å), aluminum oxide (alumina), silicon dioxide (silica) for column chromatography and silica plates for thin layer chromatography were purchased from Merck SA. Dimethylformamide (DMF) used in ligand syntheses, UV–Vis spectroscopy and electrochemical experiments was dried and stored over molecular sieves. All metal complexes and ligands were stored over P<sub>2</sub>O<sub>5</sub>. Ultrapure water was obtained from an ElgaPurelab Ultra system.

### 2.2. Equipment

FTIR spectra were recorded using a Bruker Alpha FTIR spectrometer equipped with an ATR platinum Diamond 1 reflectance accessory. NMR experiments were conducted in *d*<sup>6</sup>-DMSO using a 400 MHz Bruker NMR spectrometer. UV–Vis spectroscopy was carried out using a Perkin–Elmer Spectrum 25 containing quartz cuvettes having a path length of 1 cm. All UV–Vis spectra were recorded in *N,N'*-dimethylformamide. Melting points were recorded using a Stuart SMP3 melting point apparatus. Elemental analysis was carried out using a CHNS-O Flash 2000 Organic Elemental Analyser. Mass spectrometry (MS) was conducted in both the positive and negative modes *via* direct injection of the samples into a Waters Micromass LCT Premier MS instrument equipped with an electrospray ionization (ESI) source and a time-of-flight (TOF) mass analyzer. Single crystal X-ray diffraction (XRD) studies were conducted using a Bruker Apex Duo equipped with an Oxford Instruments Cryojet operating at 120(±2) or 100(±2) K and an Incoatec microsource operating at 30 W. The XRD experimental parameters, refinement details of the solid-state structures as well as their descriptions can be found in the online supporting information documents. Voltammetric studies were conducted using an Autolab Potentiostat equipped with a three-electrode system: a Pt or glassy carbon working electrode, a pseudo Ag|AgCl reference electrode and a Pt counter electrode. The Autolab Nova 1.7 software was used for operation of the potentiostat and data analysis. A GCE was used for all electrocatalytic experiments. Spectroelectrochemical experiments were undertaken using a Specac optically transparent thin-layer electrochemical (OTTLE) cell.

### 2.3. Electrochemical methods

All electrochemical studies on the metal complexes were conducted in deoxygenated DMF solutions containing 0.1 M equivalents of tetrabutylammoniumtetrafluoroborate (TBABF<sub>4</sub>) as a supporting electrolyte. The Pt electrode surface was regenerated between voltammetric scans by polishing over a slurry of alumina and ultra-pure water on a diamond polishing pad followed by rinsing with ultra-pure water and anhydrous DMF. The GCE was polished over alumina on Buehler and diamond polishing pads, rinsed in Millipore water and ultrasonicated in methanol (MeOH) for 2 min prior to use. Square wave voltammetry (SWV) was conducted by setting the step potential at 4 mV, the amplitude at 20 mV and the frequency at 25 Hz.

Adsorption of the MPcs onto a GCE was achieved *via* the drop-dry method. Concentrated solutions of the metal complexes were prepared in dichloromethane (DCM) and a drop of each metal

complex was transferred onto the electrode surfaces which were then dried for 1 h at 100 °C. The CMEs were rinsed with DCM, ethanol (EtOH) and ultrapure water prior to use. A 1 mM solution of L-cysteine was prepared in pH 4 buffer for electrocatalysis. Tetra-4-(7-oxy-4-trifluoromethylcoumarin phthalocyaninato)Co(II) (CoPc-cou, **5**) used in the preparation of CMEs was synthesized as previously reported [31].

### 2.4. Synthesis of 4-(tetrahydropyran-2-methoxy)phthalonitrile (**1**)

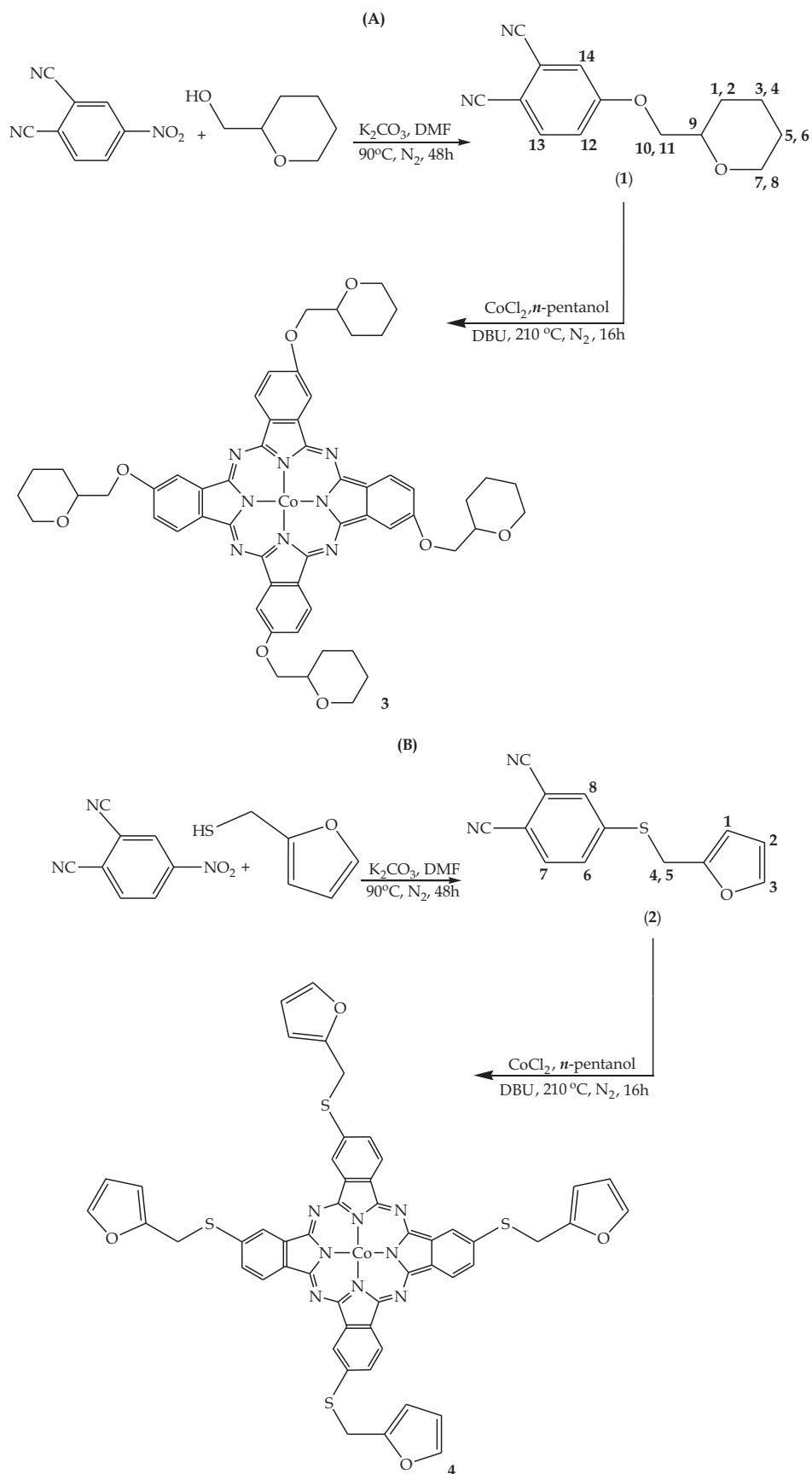
A mixture of 4-tetrahydropyran-2-methanol (0.653 cm<sup>3</sup>, 5.78 mmol) and potassium carbonate (2.30 g, 16.64 mmol) was stirred in anhydrous dimethylformamide (DMF) (30.0 cm<sup>3</sup>) at room temperature under N<sub>2</sub> for 1 h. Thereafter, to the resultant reaction mixture, 4-nitrophthalonitrile (1.00 g, 5.78 mmol) was added. The reaction mixture was removed after 48 h and poured into 300 cm<sup>3</sup> of a water–ice slurry. The resulting precipitate was filtered and purified *via* column chromatography using a 1:1 (*v:v*) ethyl acetate:hexane solvent system to produce a white compound. Yield: 20%; m.p (°C): 62.3–62.9; FT-IR ( $\nu_{\max}/\text{cm}^{-1}$ ):  $\nu(\text{C}\equiv\text{N})$  2240,  $\nu(\text{C}-\text{O}-\text{C})$  1252, 1090, 1027; UV–Vis (DMF,  $\lambda_{\max}$  ( $\epsilon$ , M<sup>-1</sup>cm<sup>-1</sup>)): 306 nm (13081), 299 (12647); <sup>1</sup>H NMR (ppm): 8.04 (d, 1H, H14), 7.78 (d, 1H, H13), 7.47 (d, 1H, H12), 4.06–4.14 (m, 2H, H10, H11), 3.85–3.92 (m, 1H, H8), 3.62–3.70 (m, 1H, H9), 3.35–3.42 (m, 1H, H7), 1.78–1.87 (m, 1H, H4), 1.59–1.67 (m, 1H, H2), 1.42–1.59 (m, 3H, H3, H5, H6), 1.26–1.38 (m, 1H, H1); <sup>13</sup>C NMR (ppm): 22.92, 25.87, 27.67, 67.74, 72.57, 75.41, 106.38, 116.20, 116.69, 116.74, 120.57, 120.83, 136.20, 162.48. Molecular mass (*m/z*): Calc.: 242.27. Found: 265.10 [M+Na]<sup>+</sup>. Anal. Calc. for C<sub>14</sub>H<sub>14</sub>N<sub>2</sub>O<sub>2</sub>: C, 69.41; H, 5.82; N, 11.56. Found: C, 64.32; H, 4.91; N, 10.73%.

### 2.5. Synthesis of 4-(furan-2-methylthio)phthalonitrile (**2**)

A mixture of 4-nitrophthalonitrile (1.00 g, 5.78 mmol), 2-furan-methanethiol (0.583 cm<sup>3</sup>, 5.78 mmol) and potassium carbonate (2.30 g, 16.64 mmol) was added to anhydrous DMF (30.0 cm<sup>3</sup>). The reaction mixture was stirred at 90 °C under N<sub>2</sub> for 48 h after which it was cooled to room temperature and poured into 300 cm<sup>3</sup> of a water–ice slurry. The resulting white precipitate was filtered and recrystallized from hot methanol (MeOH). Yield: 80%; m.p (°C): 127.8–128.5; FT-IR ( $\nu_{\max}/\text{cm}^{-1}$ ):  $\nu(\text{C}\equiv\text{N})$  2228,  $\nu(\text{C}-\text{O}-\text{C})$  1249, 1061; UV–Vis (DMF,  $\lambda_{\max}$  ( $\epsilon$ , M<sup>-1</sup>cm<sup>-1</sup>)): 323 nm (76752), 295 (137469); <sup>1</sup>H NMR (ppm): 8.15 (d, 1H, H7), 8.01 (d, 1H, H8), 7.85 (d, 1H, H6), 7.62–7.59 (m, 1H, H3), 6.42–6.38 (m, 2H, H1, H2), 4.56 (s, 2H, H4, H5); <sup>13</sup>C NMR (ppm): 28.10, 109.37, 110.73, 111.23, 115.52, 116.07, 116.49, 131.40, 131.47, 131.19, 143.58, 145.85, 149.77. Molecular mass (*m/z*): Calc.: 240.28. Found: 263.03 [M+Na]<sup>+</sup>. Anal. Calc. for C<sub>13</sub>H<sub>8</sub>N<sub>2</sub>OS: C, 64.98; H, 3.36; N, 11.66; S, 13.34. Found: C, 65.10; H, 3.36; N, 11.64; S, 13.05%.

### 2.6. Synthesis of tetra-4-(tetrahydropyran-2-methoxyphthalocyaninato)Co(II) (CoPc-thp, **3**)

A mixture of **1** (0.125 g, 0.516 mmol), CoCl<sub>2</sub> (0.0167 g, 0.129 mmol) and DBU was heated with stirring in *n*-pentanol (20.0 cm<sup>3</sup>) at 160 °C under nitrogen for 16 h. The reaction mixture was then cooled to room temperature and *n*-hexane was added drop-wise to induce precipitation. The precipitate was filtered off using a millipore filtration setup and then washed with water, MeOH, EtOH, hexane and acetonitrile. The desired product was thereafter recovered *via* column chromatography using a 1:10 (*v:v*) tetrahydrofuran (THF):CHCl<sub>3</sub> solvent system. Yield: 15%; IR ( $\nu_{\max}/\text{cm}^{-1}$ ):  $\nu(\text{C}\equiv\text{N})$  1601,  $\nu(\text{C}-\text{O}-\text{C})$  1232, 1123, 1088; UV–Vis (DMF,  $\lambda_{\max}$  ( $\epsilon$ , M<sup>-1</sup>cm<sup>-1</sup>)): 667 nm (285321), 330 nm (189512),



**Scheme 1.** Synthetic pathways for the CoPcs: (A) (CoPc-thp, **3**) and (B) (CoPc-fur, **4**).

307 (163949). Molecular mass ( $m/z$ ): Calc.: 1028.03. Found: 1027.36  $[M-H]^+$ , 1028.36  $[M]^+$ , 1029.36  $[M+H]^+$ , 1030.37  $[M+2H]^+$ . Anal. Calc. for  $C_{56}H_{56}CoN_8O_8$ : C, 65.43; H, 5.49; N, 10.90. Found: C, 65.43; H, 5.02; N, 10.60%.

### 2.7. Synthesis of tetra-4-(2-furanmethylthiophthalocyaninato)Co(II) (CoPc-fur, **4**)

The synthesis of **4** includes the addition of **2** (0.125 g, 0.520 mmol) to  $CoCl_2$  (0.0169 g, 0.130 mmol) under the specified reaction conditions of **3**. The product was washed with water, MeOH, EtOH, ethyl acetate, hexane and acetonitrile and further purified via column chromatography using a 1:10 (v:v) THF:CHCl<sub>3</sub> solvent system. Yield: 60%; IR ( $\nu_{max}/cm^{-1}$ ):  $\nu(C=N)$  1596,  $\nu(C-O-C)$  1271, 1071; UV-Vis (DMF,  $\lambda_{max}$  ( $\epsilon$ ,  $M^{-1} cm^{-1}$ )): 676 nm (161757), 331 nm (106668). Molecular mass ( $m/z$ ): Calc.: 1020.05. Found: 1019.08  $[M-H]^+$ , 1020.08  $[M]^+$ , 1021.08  $[M+H]^+$ , 1022.08  $[M+2H]^+$ . Anal. Calc. for  $C_{52}H_{32}CoN_8O_4S_4$ : C, 61.23; H, 3.16; N, 10.99; S, 12.57. Found: C, 60.65; H, 2.93; N, 10.51; S, 12.14%.

## 3. Results and discussion

### 3.1. Synthesis and spectral characterization

The <sup>1</sup>H NMR spectra of the derivatized phthalonitriles **1** and **2** are shown in Figs. S1 and S2. Both spectra contain aromatic proton peaks between 6.0 and 9.0 ppm as well as methyl proton peaks further upfield. The structures of both ligands were confirmed by X-ray crystallography, see Figs. S3 and S4. Template cyclotetramerization of ligands **1** and **2** in the presence of a catalyst, DBU and  $CoCl_2$  afforded the corresponding MPcs, refer to Scheme 1. The metal complexes displayed good solubility in low boiling point organic solvents including THF, chloroform and DCM. The FT-IR spectra of the MPcs (see Figs. S5 and S6) showed disappearance of the medium intensity nitrile stretches found at 2240  $cm^{-1}$  (for **1**) and 2228  $cm^{-1}$  (for **2**) which is typical of cyclotetramerization. In addition, the FT-IR spectra of the metal complexes display comparable  $\nu(C=N)$  stretches at 1605  $cm^{-1}$  (for **3**) and 1596  $cm^{-1}$  (for **5**). The similar ether stretches of the derivatized phthalonitriles [1252, 1090, 1027  $cm^{-1}$  for **1** and 1249, 1061  $cm^{-1}$  for **2**] and their corresponding metal complexes [1232, 1123, 1088  $cm^{-1}$  for **3** and 1271, 1071  $cm^{-1}$  for **4**] confirms the presence of the furan and tetrahydropyran moieties in **3** and **4**, respectively. ESI-TOF mass spectrometry provided definitive structural characterization for the ligands (see Figs. S7 and S8) and their metal complexes (see Figs. S9 and S10). The elemental composition of ligand **2** and the complexes were consistent with the calculated values; however the solvent molecules of **1** could not be removed from the crystals prior to elemental analysis, leading to errors. All molecular and cluster ion peaks were in accordance with the calculated  $m/z$  values. For example, the mass spectra of the MPcs showed  $[M]^+$  ion peaks at  $m/z$  values of 1028.36 (for **3**) and 1020.08 (for **4**), in addition to the protonation molecular ion peaks of the form:  $[M+H]^+$ ,  $[M+2H]^+$  and  $[M-H]^+$ .

The isolated MPcs showed Q- and B-bands in the regions of 600–700 nm and 300–400 nm, respectively, in accordance with literature [32] (see Fig. 1). The Q-bands of the metal complexes do not differ significantly in wavelength but complex **4** is slightly red-shifted due to the presence of the electron donating 2-furanmethylthiolate moieties. Both metal complexes display absorption bands in their electronic spectra that are characteristic of their corresponding ligands (refer to Table 1). The band of complex **3** appearing at 307 nm resembles the band of **1** which appears at a similar wavelength (306 nm). The broadness of the B-band of

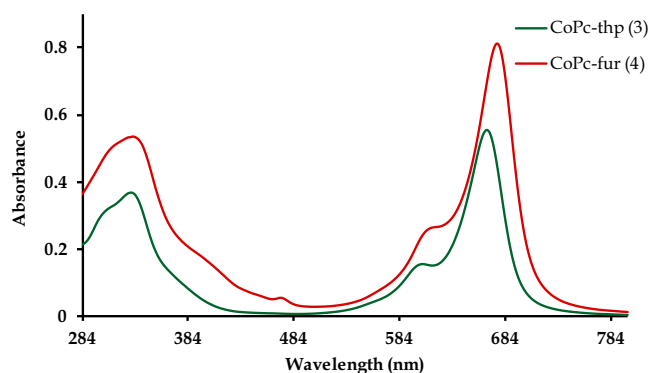


Fig. 1. UV-Vis spectra of complexes **3** and **4** at concentrations of 1.95  $\mu M$  and 5.03  $\mu M$ , respectively.

Table 1

UV-Vis absorption wavelengths and the corresponding molar absorptivities (in parentheses) for **1–4**.

Compound	Q-band (nm)	B-band (nm)	Higher energy bands (nm)
<b>1</b>	–	–	299 (12647), 306 (13081)
<b>2</b>	–	–	295 (137469), 323 (76752)
<b>3</b>	667 (285321)	330 (189512)	307 (163949)
<b>4</b>	676 (161757)	331 (106668)	–

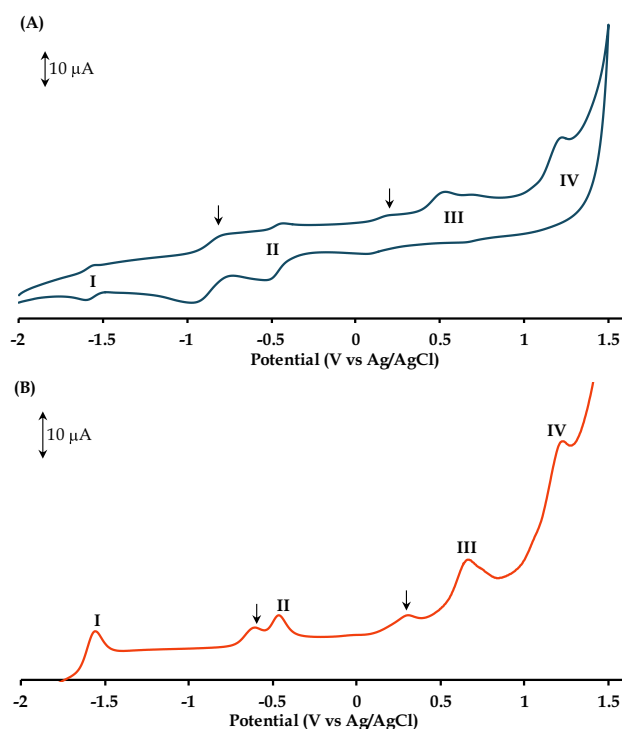
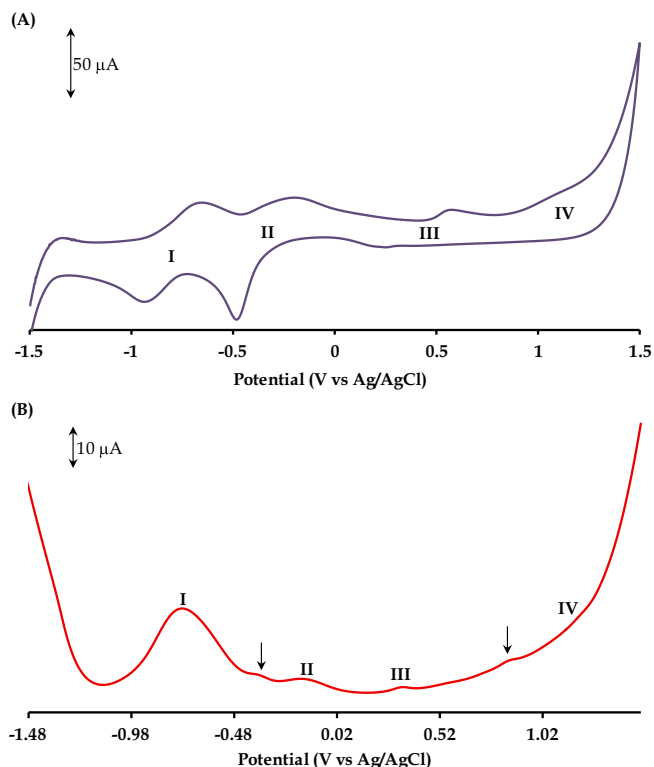


Fig. 2. (A) CV and (B) SWV of complex **3** at 100 mV/s. The arrows denote aggregate peaks.

complex **4** at 331 nm suggests that the band arises from an overlap of the  $\pi-\pi^*$  electronic transitions of the Pc ring as well as its corresponding phthalonitrile (**2**) which has an electronic transition at 323 nm.

### 3.2. Voltammetry and spectroelectrochemistry

The solution redox properties of the complexes were investigated via cyclic and square-wave voltammetry using a Pt working



**Fig. 3.** (A) CV and (B) SWV of complex **4** at 100 mV/s. The arrows denote aggregate peaks.

electrode. Both complexes **3** and **4** displayed four redox processes as observed in their respective cyclic and square-wave voltammograms, see Figs. 2 and 3. The redox couples I, II and III have larger peak to peak separations ( $\Delta E$  values) and hence exhibit slower electron transfer kinetics as compared to the ferrocene standard ( $\Delta E > 105$  mV on a Pt electrode, at 100 mV/s), thus these redox processes are considered to be quasi-reversible [33]. Redox couple IV is irreversible. The use of donor solvents in electrocatalysis is known to promote metal oxidation and reduction redox processes above Pc-based electron transfer in MPcs with redox active metal centres (e.g. Fe, Co and Mn) [33]. Hence, redox couples I to IV were assigned according to literature trends (refer to Table 2) [31,34–36]. Any unassigned peaks are attributed to aggregation. Plots of peak current against square root of scan rate for both complexes were linear indicating that the redox couples are diffusion-controlled (see Figs. 4 and S11).

Spectroelectrochemical experiments were conducted on the MPcs to verify the voltammetric assignments. The UV–Vis spectral changes of the CoPcs are similar, thus, only the

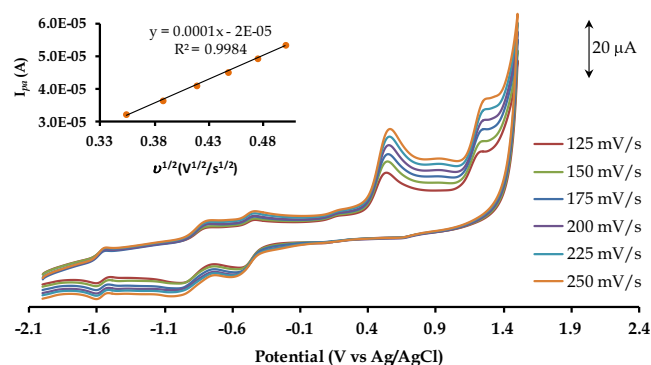


**Fig. 4.** Overlay CVs of **3** at incrementing scan rates. Inset: plot of  $I_{pa}$  against square root of scan rate (redox couple III) showing diffusion-controlled behaviour.

spectroelectrochemical data of **3** will be elaborated on. Figs. 5A–D and S12A–D illustrate the spectral changes accompanying the redox processes of complexes **3** and **4**, respectively. The *in situ* spectroelectrochemical behavior of CoPcs is well documented. It is known that a red shift in the Q-band and the formation of a CT-band between 450 and 500 nm is reminiscent of Co(I) species in solution [24,37]. Upon application of negative overpotentials to redox couple II, disaggregation and red-shifting of the Q-band occurs to produce a well-defined monomeric peak at 705 nm. Furthermore, a CT-band develops at 474 nm thereby confirming that the first redox couple occurs as a result of metal reduction ( $\text{Co}^{\text{II}}\text{Pc}^{-2}/\text{Co}^{\text{I}}\text{Pc}^{-2}$ ), see Fig. 5A. These spectral changes are accompanied by well-defined isosbestic points which are observed at 328 nm, 387 nm, 561 nm and 690 nm suggesting that the metal reduction process proceeds to afford only one species in solution.

Spectral changes associated with redox couple I include a decrease in the Q- and B-bands and a red shift of the charge transfer band to 491 nm, see Fig. 5B. This redox behavior is typical of  $\text{Pc}^{2-}$  reduction and the formation of  $\text{Pc}^{3-}$  species [38], thereby confirming that these UV–Vis spectral changes are associated with the  $\text{Co}^{\text{I}}\text{Pc}^{-2}/\text{Co}^{\text{I}}\text{Pc}^{-3}$  redox couple.

Following the application of positive overpotentials to redox couple III, considerable disaggregation accompanied by an increase in the intensity of the Q-band was observed and a new electronic transition band at 362 nm appeared. These spectral changes are consistent with metal oxidation [22]; hence the assignment of redox couple III to  $\text{Co}^{\text{II}}\text{Pc}^{-2}/\text{Co}^{\text{III}}\text{Pc}^{2-}$  is confirmed, see Fig. 5C. The spectral changes associated with redox couple IV included a decrease in the intensities of the Q-band and the band at 362 nm, see Fig. 5D. Contrary to the expectation that the redox couple IV is a Pc oxidation process based on its comparison with literature, refer to Table 2, a loss in the intensity of the Q-band with

**Table 2**

Comparison of the voltammetric data (in V) between the novel CoPcs **3** and **4** as well as other tetrasubstituted CoPcs attained from literature.

	$\text{M}^{\text{I}}\text{Pc}^{2-}/\text{M}^{\text{I}}\text{Pc}^{3-}$ I	$\text{M}^{\text{II}}\text{Pc}^{2-}/\text{M}^{\text{I}}\text{Pc}^{2-}$ II	$\text{M}^{\text{II}}\text{Pc}^{2-}/\text{M}^{\text{III}}\text{Pc}^{2-}$ III	$\text{M}^{\text{III}}\text{Pc}^{2-}/\text{M}^{\text{III}}\text{Pc}^{1-}$ IV
CoPc-thp ( <b>3</b> )	−0.870 <sup>a</sup>	−0.477 <sup>a</sup>	0.677 <sup>a</sup>	1.22 <sup>b</sup>
CoPc-fur ( <b>4</b> )	−0.796 <sup>a</sup>	−0.345 <sup>a</sup>	0.411 <sup>a</sup>	1.07 <sup>b</sup>
(β)-CoPc-ochr	−1.11	−0.44	0.40	1.03
(β)-CoPc-ofcou	−1.00	−0.46	0.42	1.08
(β)-CoPc-cfcou	−0.81	−0.47	0.48	0.91
(α)-CoPc-cfcou	−0.86	−0.35	0.42	1.00

cfcou = 7-oxo-3-(2-chloro-4-fluorophenyl)coumarin.  
ochr = 7-oxychromone.

ofcou = 7-oxy-4-trifluoromethylcoumarin.

<sup>a</sup>  $E_{1/2} = \frac{E_{ox} + E_{pc}}{2}$ .

<sup>b</sup>  $E_{pa}$ .

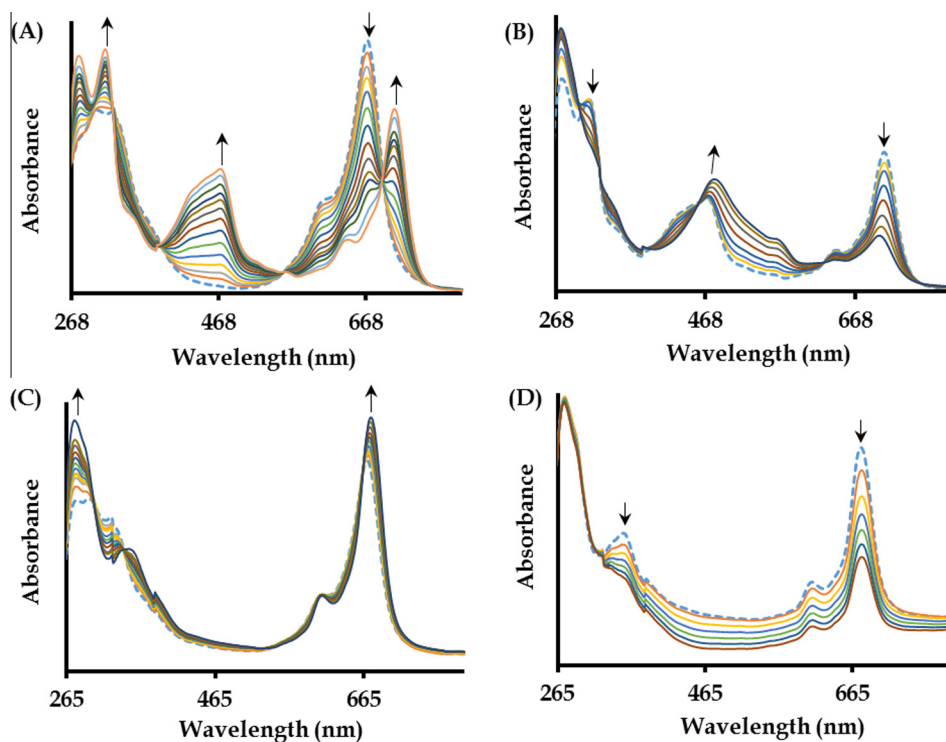


Fig. 5. UV-Vis spectral changes of complex **3** at overpotentials applied at (A)  $-0.35$  V, (B)  $-1.10$  V, (C)  $0.60$  V and (D)  $1.20$  V. The initial spectrum is shown as a dashed line.

no appreciable increase in the  $500$  nm region, suggests that progressive degradation of the MPC has occurred. This has previously been reported for cobalt complexes [39]. Redox couple **IV** is expected to be due to  $\text{Co}^{\text{III}}\text{Pc}^{2-}/\text{Co}^{\text{III}}\text{Pc}^{1-}$ .

### 3.3. Characterization of modified electrodes

Complex **4** did not show any electrocatalytic activity towards the biological analyte  $\text{l-cysteine}$  used in this study and is hence omitted from the sections that follow. Complexes **3** and **5** were adsorbed onto respective GCEs *via* the drop-dry method. CVs at incrementing scan rates were obtained for each CME in pH 4 buffer solution to confirm electrode modification, see Figs. 6 and S13. The CVs revealed broadened redox couples attributed to redox process **II** ( $\text{Co}^{\text{III}}/\text{Co}^{\text{II}}$ ) thereby corroborating modification of the GCEs.

Further confirmation of electrode modification is ascertained from the fact that the degree of ion-permeability for the modified

working electrodes is different from that of the bare electrode ( $\Delta E = 107$  mV), see Fig. 7. The surface coverages of the respective modified working electrodes were calculated from the overlay CVs using the following equation [40]:

$$I_p = \frac{n^2 F^2 A \Gamma(v)}{4RT} \quad (1)$$

where  $I_p$  is the peak current of redox couple **II**,  $n$  is the number of electrons and  $A$  is the real surface area ( $0.0707$  cm<sup>2</sup>) of the bare GCE. The surface coverage values of the modified electrodes ( $2.97 \times 10^{-10}$  mol/cm<sup>2</sup> for **3**-GCE,  $6.53 \times 10^{-10}$  mol/cm<sup>2</sup> for **5**-GCE) correspond well with surface coverage values previously obtained for a monolayer electrodeposited flat on an electrode surface ( $1 \times 10^{-10}$  mol/cm<sup>2</sup>) [41].

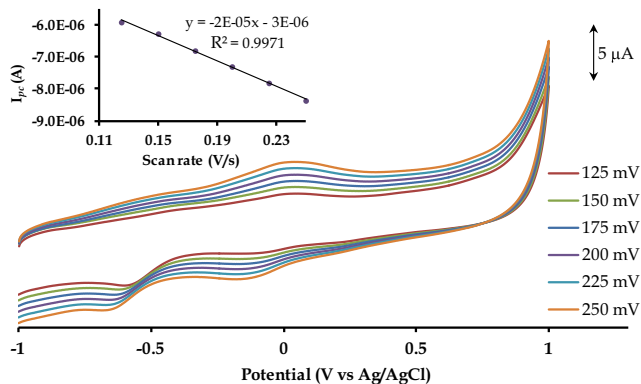


Fig. 6. Overlay CVs at incrementing scan rates of **3**-GCE in pH 4 buffer solution. Inset: the linear relationship between reduction peak currents ( $I_{pc}$ ) vs. scan rates measured at the redox couple **II**.

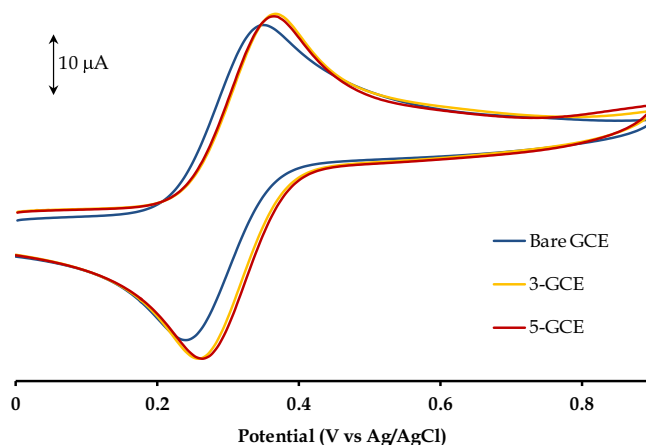
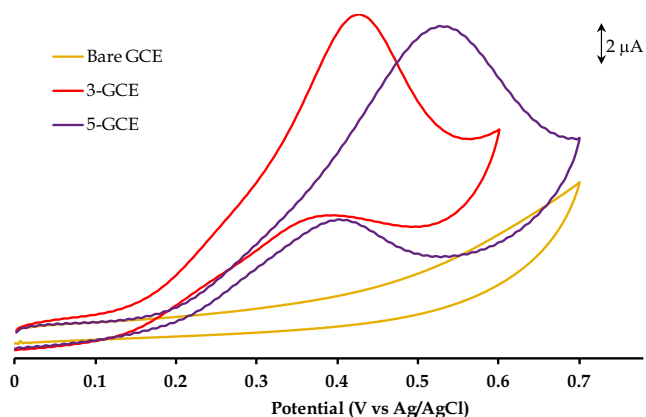


Fig. 7. Overlay CVs in  $1$  mM ferrocene of the bare electrode, **3**-GCE and **5**-GCE at  $100$  mV/s.



**Fig. 8.** Electrocatalytic oxidation of 1 mM L-cysteine in pH 4 buffer solution using the modified and bare electrodes at 100 mV/s.

### 3.4. Electrocatalysis of L-cysteine

In contrast to the modified electrodes **3**-GCE and **5**-GCE, a bare GCE does not display any oxidation peak for L-cysteine within the potential window of 0.0–0.7 V, see Fig. 8. The appearance of L-cysteine oxidation peaks at low potentials for the modified electrodes suggests that this process is promoted by the metal oxidation couple (*i.e.* Co<sup>III</sup>/Co<sup>II</sup>) which is found in the same vicinity as the electrocatalytic potential of L-cysteine using the respective modified electrodes (in pH 4 buffer).

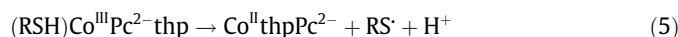
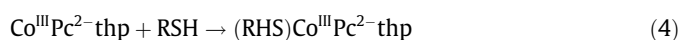
The cyclic voltammograms of the CMEs in L-cysteine show a well defined peak at 0.42 V for **3**-GCE and a broad peak at 0.52 V for **5**-GCE. In addition, the peak current for **3**-GCE is larger than **5**-GCE indicating that the former is more electrocatalytically active. A linear increase in the oxidation peak currents ( $I_{pa}$ ) with the square root of the scan rates ( $v^{1/2}$ ) was observed for the peak potentials which affirms diffusion-controlled behaviour. Furthermore, **3**-GCE and **5**-GCE show lower electrocatalytic oxidation potentials of L-cysteine compared to previously reported glassy carbon electrodes modified with peripherally ( $\beta$ ) tetra-substituted 4-(2-mercaptoquinoline phthalocyaninato)cobalt (CoPcSHQn) [ $E_{pa} = 0.62$  V] and 4-(2-phenoxy-4-trifluoromethylpyridine phthalocyaninato)cobalt (CoPcOHPy) [ $E_{pa} = 0.59$  V] as well as a gold electrode modified with CoPcSHQn [ $E_{pa} = 0.83$  V] [42]. Tafel plots (see Figs. 9 and S14) were constructed to obtain mechanistic information about the electro-

catalyzed oxidation of L-cysteine. The Tafel slopes were obtained from plots of  $E_p$  versus  $\text{Log } v$  using Eq. (2):

$$E_p = \frac{2.3RT}{2(1-\alpha)Fn_\alpha} \text{Log } v + K \quad (2)$$

where  $\alpha$  is the transfer coefficient,  $v$  is the scan rate,  $n_\alpha$  is the number of electrons in the rate-determining step and  $K$  is the intercept.

The large Tafel slopes obtained for **3**-GCE (182 mV/decade) and **5**-GCE (237 mV/decade) are outside the normal range of 30–120 mV/decade which is known to be due to substrate-catalyst interactions, where the substrate (L-cysteine) binds very strongly to the catalyst (CoPc) during oxidation [43,44]. Given that the oxidation of L-cysteine is promoted by the Co<sup>III</sup>/Co<sup>II</sup> couple, the following reaction mechanism is proposed from literature using CoPc-thp as an example [44]:



where RSH is L-cysteine and RSSR is cystine.

The presence of the furan moieties in **4** induces non-electrocatalytic behavior towards the bio-analyte, L-cysteine. In contrast, for **3**-GCE and **5**-GCE, the presence of their individual substituents promotes the electrocatalysis of L-cysteine. The different electrocatalytic potentials of L-cysteine for **3**-GCE and **5**-GCE are ascribed to the variable electron-donating capabilities of their substituents to their tetramer cores. More specifically, the electron-donating capabilities of the tetrahydropyran substituents in **3** is weaker compared to the  $\pi$ -conjugated 4-trifluoromethylcoumarin substituents in **5**.

### 3.5. Chronoamperometry studies

Chronoamperometry was used to determine the electrocatalytic rate-constants for **3**-GCE and **5**-GCE in 1 mM L-cysteine. The chronoamperograms were obtained by setting the overpotentials on the CMEs to 0.45 and 0.53 V for **3**-GCE and **5**-GCE, respectively. Figs. 10 and S15 display the chronoamperograms for the modified electrodes. At intermediate times ( $t = 0.4$ – $1.0$  s), the catalytic current is dominated by the rate of the electrocatalyzed oxidation of L-cysteine [45] and the rate constants for the chemical reaction

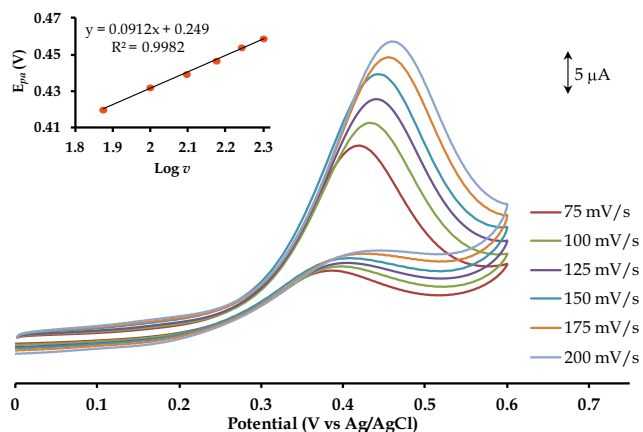


**Fig. 9.** Electrocatalytic oxidation of 1 mM L-cysteine in pH 4 buffer solution by **3**-GCE at incrementing scan rates from 75 mV/s to 200 mV/s. Inset: plot of  $E_{pa}$  vs  $\text{Log } v$ .

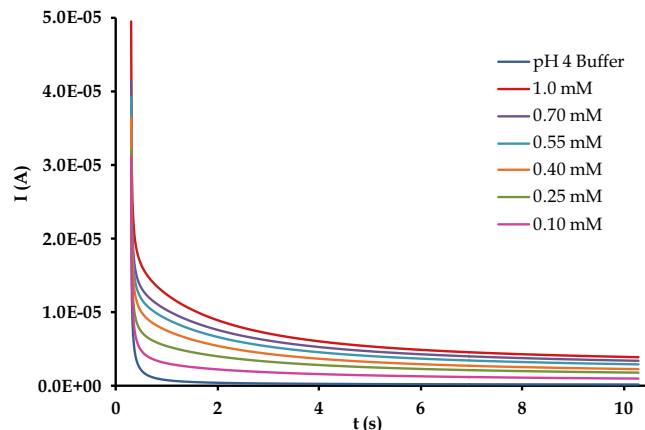


**Fig. 10.** Chronoamperograms of **5**-GCE in pH 4 buffer at different concentrations of L-cysteine.

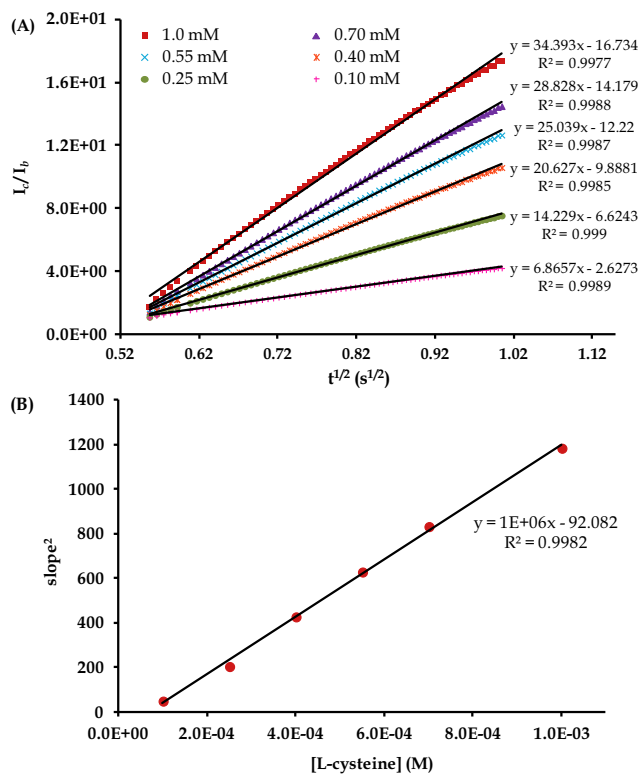


Fig. 11. (A) Plot of  $I_c/I_b$  against  $t^{1/2}$  and (B) Plot of  $\text{slope}^2$  against [L-cysteine] for 5-GCE.

between L-cysteine and the redox sites of the modifiers on the CMEs were calculated according to literature methods [46,47]:

$$\frac{I_c}{I_b} = \gamma^{1/2} \left[ \pi^{1/2} \text{erf}(\gamma^{1/2}) + \frac{\exp(-\gamma)}{\gamma^{1/2}} \right] \quad (7)$$

where  $\gamma = kC_0t$  ( $C_0$  is the bulk concentration of L-cysteine) and  $\text{erf}^{1/2}$  is the error function. In cases where  $\gamma$  exceeds 2, the error function is almost equal to 1 and the above equation reduces to:

$$\frac{I_c}{I_b} = \sqrt{\gamma\pi} = \sqrt{\pi kC_0t} \quad (8)$$

where  $I_c$  and  $I_b$  are the currents in the presence and in the absence of L-cysteine,  $t$  is the time elapsed (s) and  $k$  is the rate constant ( $\text{M}^{-1} \text{s}^{-1}$ ).

Plots of  $I_c/I_b$  against  $t^{1/2}$  (see Figs. 11A and S16A) for different concentrations of L-cysteine were constructed from the chronoamperograms. The slopes obtained from these plots were plotted against the concentration of L-cysteine to afford a linear relationship. The rate constants were subsequently determined from the slopes of Figs. 11B and S16B to be  $6.83 \times 10^5 \text{ M}^{-1} \text{ s}^{-1}$  for 3-GCE and  $3.83 \times 10^5 \text{ M}^{-1} \text{ s}^{-1}$  for 5-GCE. It can be noted that the higher surface coverage of 5-GCE produced a higher L-cysteine oxidation potential and a lower rate constant as compared to 3-GCE. The rate constants are higher than previously reported studies, e.g. indigocarmine ( $5.90 \times 10^4 \text{ M}^{-1} \text{ s}^{-1}$ ), poly(4-vinylpyridine) ( $8.95 \times 10^3 \text{ M}^{-1} \text{ s}^{-1}$ ) and tetraamino CoPc ( $2.20 \times 10^5 \text{ M}^{-1} \text{ s}^{-1}$ ) modified electrodes [48–50].

#### 4. Conclusion

CoPcs bearing tetrahydropyran and furan substituents were synthesized and spectroscopically characterized. Both CoPcs exhibited similar voltammetric behaviour. The UV–Vis spectral changes accompanying each redox couple confirmed the respective

voltammetric assignments and were comparable to those reported for similar tetrasubstituted mononuclear CoPcs. Chemically modified GCEs were prepared using CoPc-thp and the previously reported CoPc-cou via the drop-dry method. Both fabricated GCEs were found to electrocatalytically enhance the detection of L-cysteine.

#### Appendix A. Supplementary material

CCDC 1451495 and 145149 for compounds 1 and 2 contains the supplementary crystallographic data for this paper. These data can be obtained free of charge from The Cambridge Crystallographic Data Centre via [www.ccdc.cam.ac.uk/data\\_request/cif](http://www.ccdc.cam.ac.uk/data_request/cif). Supplementary data associated with this article can be found, in the online version, at <http://dx.doi.org/10.1016/j.ica.2016.04.021>.

#### References

- [1] I. Ohtsu, N. Wiriyanawudhiwong, S. Morigasaki, T. Nakatani, H. Kadokura, H. Takagi, *J. Biol. Chem.* 285 (2010) 17479.
- [2] N. Maleki, A. Safavi, F. Sedaghati, F. Tajabadi, *Anal. Biochem.* 369 (2007) 149.
- [3] R. Devasenathipathy, V. Mani, S.M. Chen, K. Kohilarani, S. Ramaraj, *Int. J. Electrochem. Sci.* 10 (2015) 682.
- [4] X. Wang, L. Zhang, L. Miao, M. Kan, L. Kong, H. Zhang, *Sci. China Chem.* 54 (2011) 521.
- [5] Z.X. Zheng, Q.L. Feng, J. Li, C.M. Wang, *Sens. Actuators, B* (2015), <http://dx.doi.org/10.1016/j.snb.2015.07.069>.
- [6] F. de Assis dos Santos Silva, M.G.A. da Silva, P.R. Lima, M.R. Meneghetti, L.T. Kubota, M.O.F. Goulart, *Biosens. Bioelectron.* 50 (2013) 202.
- [7] P.C. Pandey, A.K. Pandey, D.S. Chauhan, *Electrochim. Acta* 74 (2012) 23.
- [8] Z. Liu, H. Zhang, S. Hou, H. Ma, *Microchim. Acta* 177 (2012) 427.
- [9] J. Obirai, T. Nyokong, *Electrochim. Acta* 50 (2005) 5427.
- [10] M.K. Halbert, R.P. Baldwin, *Anal. Chem.* 57 (1985) 591.
- [11] A.T. Bilgili, A. Günsel, M. Kandaz, A. Altindal, H. Comert, *J. Organomet. Chem.* 785 (2015) 112.
- [12] K.I. Ozoemena, T. Nyokong, *Electrochim. Acta* 51 (2006) 2669.
- [13] S.L. Vilakazi, T. Nyokong, *J. Electroanal. Chem.* 512 (2001) 56.
- [14] S.B.A. Barrosa, A. Rahim, A.A. Tanaka, L.T. Arenas, R. Landers, Y. Gushikem, *Electrochim. Acta* 87 (2013) 140.
- [15] T. Nyokong, in: J.H. Zagal, F. Bedioui, J.-P. Dodelet (Eds.), *N4-Macrocylic Metal Complexes*, Springer Science + Business Media, LLC, New York, 2006, pp. 315–361 (chapter 7).
- [16] J.H. Zagal, S. Griveau, J.F. Silva, T. Nyokong, F. Bedioui, *Coord. Chem. Rev.* 254 (2010) 2755.
- [17] S. Chohan, I.N. Booyesen, A. Mambanda, *Polyhedron* 102 (2015) 284.
- [18] A.P. Gutierrez, S. Griveau, C. Richard, A. Pailleret, S. Granados, F. Bedioui, *Electroanalysis* 21 (2009) 2303.
- [19] Y. Acikbas, M. Evyapan, T. Ceyhan, R. Capan, O. Bekaroglu, *Sens. Actuators, B* 123 (2007) 1017.
- [20] K. Wang, L. Dai, Q. Liu, H. Li, C. Ju, J. Wu, H. Li, *Analyst* 136 (2011) 4344.
- [21] F. Mir Khalaf, J.E. Graves, *Chem. Pap.* 66 (2012) 472.
- [22] G. Ozgul, A. Tastemel, A.R. Ozkaya, M. Bulut, *Polyhedron* 85 (2015) 181.
- [23] M. Camur, A.A. Esenpinar, A.R. Ozkaya, M. Bulut, *J. Organomet. Chem.* 696 (2011) 1868.
- [24] M.B. Kılıçaslan, H. Kantekin, A. Koca, *Dyes Pigm.* 103 (2014) 95.
- [25] J.C. Obirai, T. Nyokong, *J. Electroanal. Chem.* 600 (2007) 251.
- [26] V. Mani, R. Devasenathipathy, S.M. Chen, S.T. Huang, V.S. Vasantha, *Enzyme Microb. Technol.* 66 (2014) 60.
- [27] K. Manna, Y.K. Agrawal, *Bioorg. Med. Chem.* 19 (2009) 2688.
- [28] L. Ignatovich, V. Romanov, J. Spura, J. Popelis, I. Domracheva, I. Shestakova, *Chem. Heterocycl. Compd.* 47 (2012) 1502.
- [29] J.V. Kosaric, D.M. Cvetkovic, M.N. Zivanovic, M.G. Curcic, D.S. Seklic, Z.M. Bugarcic, S.D. Markovic, *JBUON* 19 (2014) 283.
- [30] K. Akiyama, S. Yamauchi, M. Maruyama, T. Sugahara, T. Kishida, Y. Koba, *Biosci. Biotechnol. Biochem.* 73 (2009) 129.
- [31] S. Chohan, I.N. Booyesen, A. Mambanda, M.P. Akerman, *J. Coord. Chem.* 68 (2015) 1829.
- [32] N. Sehlotho, M. Durmus, V. Ahsen, T. Nyokong, *Inorg. Chem. Commun.* 11 (2008) 479.
- [33] B. Koksoy, O. Soyer, E.B. Orman, A.R. Ozkaya, M. Bulut, *Dyes Pigm.* 118 (2015) 166.
- [34] S. Altun, A.R. Ozkaya, M. Bulut, *Polyhedron* 48 (2012) 31.
- [35] A. Alemdar, A.R. Ozkaya, M. Bulut, *Polyhedron* 28 (2009) 3788.
- [36] Z. Odabaş, H. Kara, A.R. Ozkaya, M. Bulut, *Polyhedron* 39 (2012) 38.
- [37] I.A. Akinbulu, T. Nyokong, *Polyhedron* 28 (2009) 2831.
- [38] V. Cakir, H. Kantekin, Z. Bilyiklioglu, A. Koca, *Polyhedron* 81 (2014) 525.
- [39] B. Agboola, K.I. Ozoemena, T. Nyokong, *Electrochim. Acta* 51 (2006) 4379.
- [40] A. Maringa, E. Antunes, T. Nyokong, *Electrochim. Acta* 121 (2014) 93.
- [41] F. Matemadombo, T. Nyokong, *Electrochim. Acta* 52 (2007) 6856.
- [42] A. Erdoğan, I.N. Booyesen, T. Nyokong, *Synth. Met.* 161 (2011) 241.

- [43] F. Bedioui, S. Griveau, T. Nyokong, A.J. Appleby, C.A. Caro, M. Gulppi, G. Ochoa, J.H. Zagal, *Phys. Chem. Chem. Phys.* 9 (2007) 3383.
- [44] N. Sehlotho, T. Nyokong, *Electrochim. Acta* 51 (2006) 4463.
- [45] T. Mugadza, T. Nyokong, *Electrochim. Acta* 56 (2011) 1995.
- [46] J.B. Raof, R. Ojani, H. Beitollahi, *Int. J. Electrochem. Sci.* 2 (2007) 534.
- [47] M.H. Pournaghi-Azar, R. Sabzi, *J. Electroanal. Chem.* 543 (2003) 115.
- [48] M. Mazloum-Ardakani, H. Rajabi, H. Bietollahi, *J. Argent. Chem. Soc.* 97 (2009) 106.
- [49] C.C. Correa, S.A.V. Jannuzzi, M. Santhiago, R.A. Timm, A.L.B. Formiga, L.T. Kubota, *Electrochim. Acta* 113 (2013) 332.
- [50] S. Nyoni, T. Mugadza, T. Nyokong, *Electrochim. Acta* 128 (2014) 32.